Electron Localization and the Structure of Transition-Metal Chains

Stephen Lee

Contribution from the Department of Chemistry, The University of Michigan, Ann Arbor, Michigan 48109-1055. *Received March 9, 1989*

Abstract: We describe the modifications induced in a molecular orbital model of transition-metal clusters by the inclusion of electron localization. We show that while for $(t_{2g})^1$ configurations the molecular orbital predictions are left unaltered by electron localization, such is not the case for $(t_{2g})^3$ configurations.

Work of the last few years has shown that extended Hückel (eH) calculations can be a powerful tool in rationalizing crystal structure types. Indeed, the wide range of materials that have been treated using this method is remarkable. The reported calculations range from those on halides, oxides, chalcogenides, pictinides, carbides, and borides all the way to alloys and elemental structures.[1] In many cases, the researchers have used the eH method in a similar manner. The authors compare a series of related structure types and then proceed to show why at certain electron counts (i.e., for a given number of electrons per atom or per unit cell) one specific structure is found to be energetically preferred. In certain comparisons the eH calculations exactly predict the critical electron count at which structures change from one type to another. Examples of such gratifying accurate predictions are to be found in the correct sorting among the binary transition-metal oxides of the sphalerite, TiO, NbO, and PdO structure types, among the metal hydride chlorides of the CaHCl, GdHCl, and ZrHCl structure types, among the bottom-row main-group elements of the hexagonal closed-packed, face-center cubic, α-Bi and α-Po structure types, and among transition-metal binary alloys of the CsCl and CuTi structure types.[2] The above list is by no means complete but does illustrate the sorts of systems for which the eH method appears to be at its most reliable.

Equally of interest though are those systems for which the eH method gives results of only approximate validity. One example of such approximate validity[3] is found when comparing the rutile,

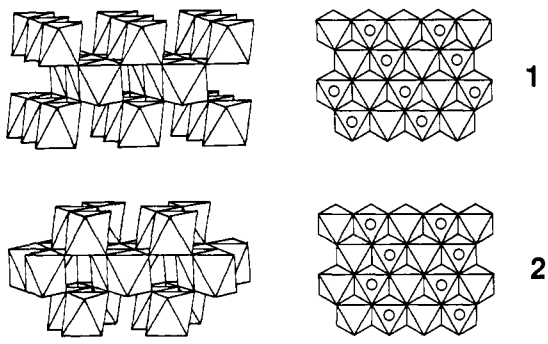

1, and α-PbO_2, **2**, structures. The eH calculations for d^0 through d^6 transition-metal dioxides are shown in Figure 1. When comparing the predictions shown in Figure 1 with the known experimental facts, one finds generally good agreement only for low d electron counts. For example, the eH calculation predicts only a small energy difference between the two types for a d^0 transition metal and indeed TiO_2 is known in both the rutile and the α-PbO_2 structure types. (ZrO_2 and HfO_2 have an entirely different coordination around the metal atoms.) Similarly the eH calculations are accurate for d^1 systems. As Figure 1 shows, the rutile structure is preferred and indeed VO_2, NbO_2, and TaO_2 are all found in the rutile or the Peierl's distorted rutile structure, **3**.[4]

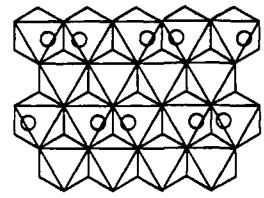

3

It is for the transition-metal dioxides near the half-filled t_{2g} band for which the extended Hückel calculations deviate from experimental results. For d^2 and d^4 transition-metal systems the rutile or distorted rutile structures are invariably found, while the calculations indicate α-PbO_2 is the preferred structure. For d^3 transition-metal systems such as ReO_2 the eH method predicts that ReO_2 should be in the α-PbO_2 structure type. The difference in energies for the undistorted structures is a hefty 0.4 eV/metal atom (see Figure 1). The ReO_2 system is therefore expected to be found only in the α-PbO_2 structure type. In reality ReO_2 is found in both forms with α-ReO_2 belonging to the rutile type and β-ReO_2 belonging to the α-PbO_2 type. We see therefore that the energetics for the d^3 ReO_2 system must be closer to that found in the d^0 TiO_2 system than the eH calculations would have led one to believe.

The source of this deviation is understandable. It is known, for example, that the spectra of d^2 and d^3 transition-metal species are dominated by their multiplet structure. This multiplet structure is due to electron–electron repulsion, which is ignored in the eH method. A second effect is electron localization.[5] It

(1) (a) Li, J.; Hoffmann, R. J. *Phys. Chem.* **1988**, *92*, 487. (b) Canadell, E.; Mathey, Y.; Whangbo, M. H. *J. Am. Chem. Soc.* **1988**, *110*, 104. (c) Burdett, J. K.; Coddens, B. A. *Inorg. Chem.* **1988**, *27*, 418. (d) Zheng, C.; Hoffmann, R.; Nesper, R.; von Schnering, H. G. *J. Am. Chem. Soc.* **1986**, *108*, 1876. (e) Tremel, W.; Hoffmann, R.; Silvestre, J. *J. Am. Chem. Soc.* **1986**, *108*, 5174. (f) Wheeler, R. A.; Whangbo, M. H.; Hughbanks, T.; Hoffmann, R.; Burdett, J. K.; Albright, T. A. *J. Am. Chem. Soc.* **1986**, *108*, 2222. (g) Burdett, J. K.; Miller, G. J. *J. Am.* Chem. *Soc.* **1987**, *109*, 4081. (h) Bernstein, J.; Hoffmann, R. *Inorg. Chem.* **1985**, *24*, 4100. (i) Burdett, J. K.; Canadell, E.; Hughbanks, T. *J. Am. Chem. Soc.* **1986**, *108*, 3971.

(2) (a) Burdett, J. K.; Hughbanks, T. *J. Am. Chem. Soc.* **1984**, *106*, 3101. (b) Burdett, J. K.; Miller, G. J. *J. Am. Chem. Soc.* **1987**, *109*, 4092. (c) Burdett, J. K.; McLarnan, T. J. *J. Solid State Chem.* **1984**, *53*, 382. (d) Burdett, J. K.; Lee, S. *J. Am. Chem. Soc.* **1985**, *107*, 3063.

(3) Burdett, J. K. *Struct. Bonding (Berlin)* **1987**, *65*, 29.

(4) A discussion of the distorted rutile structure found in transition-metal oxides can be found in: Kepert, D. L. *The Early Transition Metals*; Academic Press: New York, 1972; pp 190–193.

(5) (a) Classic accounts of the effects of electron localization may be found in: Anderson, P. W. In *Magnetism*; Rado, G., Suhl, H., Ed.; Academic Press: New York, 1963; Vol. 1. Ziman, J. M. *Principles of the Theory of Solids*; Cambridge University Press: Cambridge, 1965; Chapter 5. More recent studies include: (b) Said, M.; Maynau, D.; Malrieu, J.-P.; Garcia Bach, M.-A. *J. Am. Chem. Soc.* **1984**, *106*, 571. (c) Said, M.; Maynau, D.; Malrieu, J.-P. *J. Am. Chem. Soc.* **1984**, *106*, 580. (d) Herrick, D. R. *J. Chem. Phys.* **1981**, *74*, 1239. (e) Alexander, S. A.; Klein, D. J. *J. Am. Chem. Soc.* **1988**, *110*, 3401. (f) Klein, D. J.; Nelin, C.; Alexander, S.; Matsen, F. A. *J. Chem. Phys.* **1982**, *77*, 3101. (g) Borden, W. T.; Davidson, E. R. *J. Am. Chem. Soc.* **1977**, *99*, 4587. (h) Ovchinnikov, A. A. *Theor. Chim. Acta* **1978**, *47*, 297. (i) Cizek, J.; Pauncz, R.; Vrscay, E. R. *J. Chem. Phys.* **1983**, *78*, 2468. (j) Bondeson, S. R.; Soos, Z. G. *J. Chem. Phys.* **1979**, *71*, 3807. (k) Gautier, F. In *Magnetism of Metals and Alloys*; Cyrot, M., Ed.; North-Holland: Amsterdam, 1982. (l) Kaplan, T. A.; Horsch, P.; Fulde, P. *Phys. Rev. Lett.* **1982**, *49*, 889. (m) Lee, S. *J. Chem. Phys.* **1989**, *90*, 2732 and 2741.

0002-7863/89/1511-7754$01.50/0

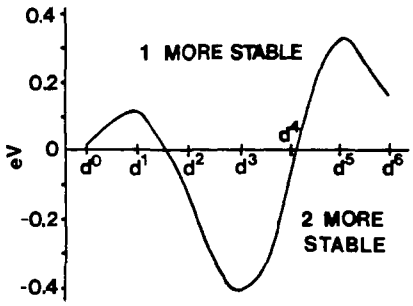

Figure 1. Differences in energy between the rutile structure type, **1**, and the α-PbO_2 type, **2**, as a function of the number of d electrons. This curve is reproduced with permission of the author: Burdett, J. K. *Struct. Bonding* **1987**, *65*, 29. Positive values of the plotted curve indicate that **1** (rutile) is lower in energy while negative values indicate α-PbO_2 is more stable. The calculations reproduced here were done for a MoO_2 stoichiometry.

is known that the magnetic susceptibility of coupled d^3 octahedral systems can be quantitatively accounted for with the spin Hamiltonian

$$H = -\sum_{k \neq l} J_{kl} \vec{S}_k \cdot \vec{S}_l \qquad (1)$$

where we fix a $^3/_2$ spin particle with corresponding spin operator $\vec{S}$ at each metal position.[6] This electron localization is again caused by electron–electron repulsion and is again not considered in the eH method. We show in this paper that the inclusion of these two effects does not alter the correct eH predictions for the d^1 systems but does alter the prediction for the d^3 case. We shall see that, for the latter systems, the effect of extreme localization is to eliminate all differences between the energies of the rutile and α-PbO_2 structure types. This corresponds well with the known α- and β-ReO_2 structures and other related structural questions.

Hubbard Model. Configuration interaction (which is the mixing of different Slater determinants to produce a composite ground state) is generally introduced as a perturbative correction to a good Hartree–Fock or semiempirical calculation.[7] Our interest though is in studying the effect of electron localization. This requires at the outset the inclusion of configuration interaction (CI). That this is so may be seen by the following argument: Systems that are extremely localized have a fixed number of electrons at each atomic site. In order for an electron to migrate from one site to another, it must therefore exchange positions with another electron (hence, the name of *exchange* parameter for the J in eq 1). Complete localization therefore implies complete correlated motion of the electrons. Correlated electronic motion though is just CI.

The simplest Hamiltonian, which includes CI, is that of eq 1. Our interest though is in correlating this spin Hamiltonian with the molecular orbital models, which have been used very effectively in solid-state systems. The simplest way of doing so is through the Hubbard Hamiltonian[8]

$$H_{\text{Hubbard}} = \sum_{\substack{k>l \\ \alpha}} \beta_{kl} a^+_{k\alpha} a_{l\alpha} + U \sum_l a^+_{l+} a^+_{l-} a_{l-} a_{l+} \qquad (2)$$

(see Table I for the symbol key.) The Hubbard Hamiltonian considers two separate forces. The first force is the β interaction of Hückel theory; the second is the intraatomic electron–electron repulsion, U. This Hamiltonian has both the Hückel and spin Hamiltonians as asymptotic cases. It is well suited for systems that have localized one electron per atomic orbital. However, we are interested in the d^1 and d^3 octahedral transition-metal systems (d^2 systems are numerically somewhat intractractable). For d^1 metals we have localization of one electron per three atomic orbitals (i.e., the t_{2g} set). Similarly, for d^3 systems we need to consider the multiplet structure (as found for example in a Tanabe–Sugano diagram[9]). We therefore must, like many others, alter the Hubbard Hamiltonian to suit our particular needs.

Finally we point out that a major assumption of the Hubbard model is that the dominant interatomic interaction is the Hückel β interaction. This interaction produces chemical bonds, and it therefore corresponds to antiferromagnetic coupling between atoms. Ferromagnetic interactions can be created (in our Hubbard type model) but only through the inclusion of intramolecular Hund's rule effects (examples of this are found in mixed-valence compounds,[10] donor–acceptor systems,[11] and the 90° bond angle interaction of the Goodenough rules[12]). Thus, when we apply our results to structural questions, we must limit ourselves to those systems where the β interaction is the dominant interatomic pathway.

Table I. Symbol Key

a and a^+	annihilation and creation operators
k,l,k',l'	atom indices
ξ, η, ζ	t_{2g} orbitals
u, v	e_g orbitals
i, j, i', j'	t_{2g} indices
m, n	electron spin indices: up spin is (+), down spin is (−)
H_{gH}, $H_{Hückel}$	generalized Hubbard and Hückel Hamiltonians
H_{loc} (K/J)	localized limit of H_{gH} as a function of K/J
$\Psi_{Hückel}$, Ψ_{loc} (K/J)	ground state of their respective Hamiltonians
$\lvert\zeta_k\bar{\xi}_l\rvert$	refers to the Slater determinant $\begin{vmatrix}\zeta_{k+}(r_1) & \xi_{l-}(r_1)\\ \zeta_{k+}(r_2) & \xi_{l-}(r_2)\end{vmatrix}$
P	projection on to localized space, e.g., $P\lvert\zeta_1\bar{\xi}_2\rvert + \lvert\zeta_1\bar{\xi}_1\rvert = \lvert\zeta_1\bar{\xi}_2\rvert$ for a system comprised of two (t_{2g}) metal atoms
ϕ, Ψ	molecular orbitals, ϕ_0 is the lowest energy; molecular orbital, ϕ_1 the next to lowest, etc.

$(t_{2g})^3$ Generalized Hubbard Model. As we discuss in Appendix I, the generalized Hubbard Hamiltonian, which includes intraatomic multiplet effects, is

$$H_{gH} = \sum_{\substack{j,l \\ j',l' \\ m}} \beta_{jl,j'l'} a^+_{jlm} a_{j'l'm} + \sum_l H_l \qquad (3)$$

where H_l is defined in Appendix I. The H_l terms replace the second term of eq 2 of the ordinary Hubbard model. It is the H_l term that contains the transition-metal intraatomic electron–electron interaction. This Hamiltonian quickly grows to unwieldy size. For four $(t_{2g})^1$ atoms it represents a 71280-dimensional problem while for four $(t_{2g})^3$ atoms it corresponds to a 1.3×10^7-dimensional matrix. We are therefore constrained to considering its asymptotic limits. As in the ordinary Hubbard model there are two asymptotic cases of general interest. In the delocalized regime the first term of (3) dominates while the second term is merely perturbative. This corresponds to the case where standard molecular orbital theory is certainly valid. [In the absence of the second term of (3), eq 3 becomes the Hückel Hamiltonian.] In the localized regime, the roles of the two terms is reversed. We show in Appendix I that, in the case of $(t_{2g})^3$ atoms, eq 3 reduce up to an additive constant to the form of eq 1. The exchange parameter J_{kl} is proportional to the average interatomic Hückel β^2 interaction between the k and l metal sites.

(6) See discussion of Cr(III) chains in: Hatfield, W. E.; Estes, W. E.; Marsh, W. E.; Pickens, M. W.; ter Haar, L. W.; Weller, R. R. In *Extended Linear Chain Compounds*; Miller, J. S., Ed.; Plenum: New York, 1983; Vol. 3.

(7) See discussion in: Szabo, A.; Ostlund, N. S. *Modern Quantum Chemistry*; MacMillan: New York, 1982.

(8) (a) Hubbard, J. *Proc. R. Soc. London* **1963**, *A266*, 238; *Ibid.* **1964**, *A277*, 237; *Ibid.* **1964**, *A281*, 401. (b) Hirsch, J. E. *Phys. Ref.* **1985**, *B31*, 4403. (c) Hirsch, J. E.; Sugar, R. L.; Scalapino, D. J.; Blankenbecker, R. *Phys. Rev.* **1982**, *B26*, 5033.

(9) (a) Sugano, S.; Tanabe, Y.; Kamimura, H. *Multiplets of Transition Metal Ions in Crystals*; Academic: New York, 1970. (b) Griffith, J. S. *The Theory of Transition Metal Ions*; University Press: Cambridge, 1964.

(10) Munck, E.; Papafthymiou, V.; Surerus, K. K.; Girerd, J. J. *Metal Cluster in Proteins*; Que, L., Jr., Ed.; ACS Symposium Series 372; American Chemical Society: Washington, DC; 1988; Chapter 15.

(11) Miller, J. S.; Epstein, A. J.; Reiff, W. M. *Chem. Rev.* **1988**, *88*, 201.

(12) Goodenough, J. B. *Magnetism and the Chemical Bond*; Interscience: New York, 1963.

Table II. Binary and Some Ternary Oxide and Chloride Octahedral Chain Structures

electron confign of transition metal	compsn	structure type: zigzag chain (**4**)	structure type: trans chain (**5**)	ref
d^0	TiO_2	α-PbO_2	rutile	13a
	$ZrCl_4$	$ZrCl_4$		4
	$HfTiO_4$	α-PbO_2		13b
	$ZrTiO_4$	α-PbO_2		13b
	$AlTaO_4$		rutile	13c
	$NiNb_2O_6$	columbite	rutile	13d
	$ZnTa_2O_6$	tri-α-PbO_2		13e
	$ZnNb_2O_6$	columbite		13e
d^1	VO_2		distorted rutile	4
	NbO_2		distorted rutile	4
	TaO_2		rutile	4
	$NbCl_4$		$NbCl_4$	4
	$TaCl_4$		$NbCl_4$	4
d^2	CrO_2		rutile	4
	MoO_2		distorted rutile	4
	WO_2		distorted rutile	4
	$MoCl_4$		$NbCl_4$	4
	WCl_4		$NbCl_4$	4
d^3	MnO_2		rutile	4
	TcO_2		distorted rutile	4
	ReO_2	α-PbO_2	distorted rutile	4
	$TcCl_4$	$TcCl_4$		13f
	$Cu_2Mn_3O_8$	$Cu_2Mn_3O_8$		13g

This is important, for it may be seen that in the asymptotic limit of localized behavior for $(t_{2g})^3$ atoms all memory is lost of the relative spatial orientation of second nearest neighbors. One therefore makes the following distinction between the delocalized and localized limits. In the delocalized limit one often ignores all but first nearest neighbors (as is done in simple Hückel theory). Even in the absence of direct interaction between second nearest neighbors, the second nearest neighbors can play a strong indirect role. Such is the case for the α-PbO_2 versus rutile calculations shown in Figure 1. In the localized limit on the other hand, in the absence of direct second nearest neighbor interactions, the localized Hamiltonians for α-PbO_2 and rutile become completely identical. In this localized limit, the infinite chains of edge-sharing metal octahedra **4** and **5** are of identical energy. We therefore expect that localization removes the energy difference between **4** and **5** and that hence the $(t_{2g})^3$ configuration energetically resembles the $(t_{2g})^0$ configuration.

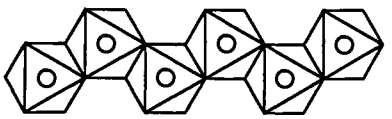

4

5

In Table II,[13] we contrast the existence of zigzag chains such as **4** with trans chains such as **5**. We consider systems where the metals are in high oxidation states and where the anions are very electronegative. It is for these cases that we expect electron localization to dominate. It may be seen that, for $(t_{2g})^3$ systems in both the MCl_4 and MO_2 (M is a transition metal) families, there appears to be no preference for either **4** or **5**. Finally, in the case of the MO_2 family, in addition to edge sharing between metal octahedra there is also vertex sharing (see **1** and **2**). We therefore need to verify that it is the interaction of edge-sharing metals that predominates. One method of doing so is to study the form of the Peierl's distortion. The direction of the Peierl's distortion indicates which metal–metal interaction is of the greatest importance. As it is found that the Peierl's pairing always occurs between edge-sharing metals, we conclude that edge interactions dominate (extended Hückel calculations bear this out). We therefore may safely apply our comparison of **4** and **5** to the question of the relative stability of α-PbO_2 versus rutile.

$(t_{2g})^3$ Wave Functions. In an earlier paper we pointed out that a strong similarity exists between the localized portion of the Hückel ground state ($P\Psi_{Hückel}$) and the ground state of the spin Hamiltonian for the corresponding system. Our earlier work was concerned with spin $^1/_2$ systems, and unfortunately our results do not carry over to the half filled $(t_{2g})^3$ case. We illustrate this by considering the bimetallic system **6**. For the sake of simplicity

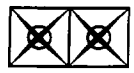

6

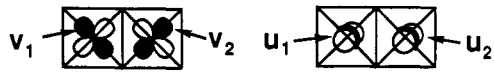

7 **8**

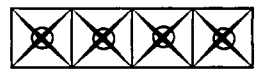

9

we consider the half-filled $(e_g)^2$ configuration in lieu of $(t_{2g})^3$. We therefore consider the four-electron system where electrons lie in the d_{z^2} (u) and the $d_{x^2-y^2}$ (v) orbitals, **7** and **8**. The $(e_g)^2$ ground-state multiplet is of $^3A_2$ symmetry, and it may therefore be treated as a spin 1 particle. The ground state of the generalized Hubbard model in the localized limit is a singlet. By symmetry is has the form

$$\Psi_{loc} = |u_1v_1\bar{u}_2\bar{v}_2| + |\bar{u}_1\bar{v}_1u_2v_2| - \tfrac{1}{2}|u_1\bar{v}_1u_2\bar{v}_2| - \tfrac{1}{2}|u_1\bar{v}_1\bar{u}_2v_2| - \tfrac{1}{2}|\bar{u}_1v_1u_2\bar{v}_2| - \tfrac{1}{2}|\bar{u}_1v_1\bar{u}_2v_2| \quad (4)$$

The Hückel ground state is of the form

$$\Psi_{Hückel} = |\phi_0\phi_1\bar{\phi}_0\bar{\phi}_1| \quad (5)$$

where

$$\phi_0 = v_1 + v_2 \quad (6)$$

$$\phi_1 = u_1 + u_2 \quad (7)$$

Therefore when we project $\Psi_{Hückel}$ onto a space where each orbital is singly occupied

$$P\Psi_{Hückel} = P|\phi_0\phi_1\bar{\phi}_0\bar{\phi}_1| = |u_1v_1\bar{u}_2\bar{v}_2| + |\bar{u}_1\bar{v}_1u_2v_2| - |u_1\bar{v}_1\bar{u}_2v_2| - |\bar{u}_1v_1u_2\bar{v}_2| \quad (8)$$

It may be seen that the resemblance between $P\Psi_{Hückel}$ and Ψ_{loc} is slight.

This result is generally true. Except in the case of spin $^1/_2$ particles, the half-filled block localized configuration (i.e., $(e_g)^2$ or $(t_{2g})^3$) bears little resemblance to the projection onto localized space of $\Psi_{Hückel}$. Indeed, it is this lack of resemblance that is responsible for the lack of correlation between $H_{Hückel}$ and H_{loc} predictions for the $(t_{2g})^3$ configuration of octahedral chains.

$(t_{2g})^1$ Generalized Hubbard Model. Unlike for the $(t_{2g})^3$ configuration, when each transition metal has only one t_{2g} electron, the generalized Hubbard model (see eq 3) does *not* become an ordinary spin Hamiltonian (see eq 1) in the limit of extreme localization. That this is so may be seen by the following argument. Each $(t_{2g})^1$ metal has a $^2T_{2g}$ multiplet ground state. The electron is not forced to be localized on any particular t_{2g} orbital

(13) (a) Villars, P.; Calvert, L. D. *Pearson's Handbook of Crystallographic Data for Intermetallic Phases*; American Society for Metals: Metals Park, Ohio, 1985. (b) Roy, R.; Muller, O. *The Major Ternary Structural Families*; Springer-Verlag: New York, 1974. (c) Jasper Tönnies, B.; Müller-Buschbaum, H. K. *Z. Anorg. Allg. Chem.* **1983**, *504*, 113. (d) Wichmann, R.; Müller-Buschbaum, H. K. *Z. Anorg. Allg. Chem.* **1983**, *503*, 101. (e) Waburg, M.; Müller-Buschbaum, H. K. *Z. Anorg. Allg. Chem.* **1984**, *508*, 55. (f) Wells, A. F. *Structural Inorganic Chemistry*, ed.; Clarendon Press: Oxford, 1975. (g) Riou, A.; Lecerf, A. *Acta Crystallogr.* **1977**, *B33*, 1896.

Table III. Comparison of Localized Portion of $\Psi_{\text{Hückel}}$ to Ψ_{loc} (K/J) for **9**[a]

	$P\Psi_{\text{Hückel}}$[b]	Ψ_{loc} $(K/J = 0.0)$	Ψ_{loc} $(K/J = 0.1)$
$\eta\eta\bar{\eta}\bar{\eta}$[c]	0.000	0.000	0.022
$\eta\eta\bar{\zeta}\bar{\zeta}$	0.000	0.000	−0.001
$\eta\bar{\eta}\eta\bar{\eta}$	0.000	0.000	0.019
$\eta\bar{\eta}\bar{\eta}\eta$	0.000	0.000	−0.041
$\eta\bar{\eta}\zeta\bar{\zeta}$	1.000	0.932	0.538
$\eta\bar{\eta}\bar{\zeta}\zeta$	−1.000	−0.932	−0.537
$\eta\zeta\bar{\eta}\bar{\zeta}$	1.000	0.933	0.973
$\eta\zeta\bar{\eta}\bar{\zeta}$[d]	1.000	1.000	1.000
$\eta\bar{\zeta}\eta\bar{\zeta}$	0.000	0.000	−0.196
$\eta\bar{\zeta}\bar{\eta}\zeta$	−1.000	−0.933	−0.777
$\eta\bar{\zeta}\zeta\bar{\eta}$	−1.000	−1.000	−0.802
$\eta\zeta\bar{\zeta}\eta$	0.000	0.000	−0.198
$\zeta\eta\bar{\eta}\bar{\zeta}$	1.000	0.871	0.912
$\zeta\eta\bar{\eta}\bar{\zeta}$	1.000	0.933	0.973
$\zeta\bar{\eta}\eta\bar{\zeta}$	−1.000	−0.871	−0.720
$\zeta\bar{\eta}\bar{\eta}\zeta$	0.000	0.000	−0.192
$\zeta\bar{\eta}\zeta\bar{\eta}$	0.000	0.000	−0.196
$\zeta\bar{\eta}\bar{\zeta}\eta$	−1.000	−0.933	−0.777
$\zeta\zeta\bar{\eta}\bar{\eta}$	0.000	0.000	−0.001
$\zeta\zeta\bar{\zeta}\bar{\zeta}$	0.000	0.000	0.018
$\zeta\bar{\zeta}\eta\bar{\eta}$	1.000	0.932	0.538
$\zeta\bar{\zeta}\bar{\eta}\eta$	−1.000	−0.932	−0.537
$\zeta\bar{\zeta}\zeta\bar{\zeta}$	0.000	0.000	0.031
$\zeta\bar{\zeta}\bar{\zeta}\zeta$	0.000	0.000	−0.049

[a] We report the values of the various ground states at $|S_\pi/S_\sigma| = 0.7$ and $S_\delta = 0$. [b] We present the ground states in column vector form. [c] The first row is the coefficient of the $|\eta_1\eta_2\bar{\eta}_3\bar{\eta}_4|$, the second row $|\eta_1\eta_2\bar{\zeta}_3\bar{\zeta}_4|$, etc. [d] We have fixed the value of the largest coefficient to 1.0.

Table IV. Overlap between Different Ground States

	$\langle P\Psi_{\text{Hückel}}\|\Psi_{\text{loc}}(K/J)\rangle$	
system	$K/J = 0.0$	$K/J = 0.1$
9	0.980	0.673
11	0.970	0.754

but rather may lie in any linear combination of the three t_{2g} orbitals. Therefore, no simple spin $^1/_2$ spin Hamiltonian of the type given in eq (1) can generate the correct number of wave functions for the couplings of the $^2T_{2g}$–$^2T_{2g}$ interatomic interactions. This is important. As the $(t_{2g})^1$ localized limit is not of the form of eq 1, energetic differences due to bond angle effects may well be retained. Such is indeed the case. In the localized limit there are two important parameters (see Appendix I) that govern electron–electron interactions. The first is the J coulombic interaction, which corresponds to the cost in energy of bringing two electrons onto one atom. It replaces the U parameter of ordinary Hubbard theory. Thus states that have an unequal number of electrons on each metal lie higher in energy than those with a uniform distribution of electrons. As we are interested in the limit of extreme localization, we need to consider only the lowest lying of these excited states. In the lowest lying excited states there is a single metal that has a $(t_{2g})^2$ configuration and another metal that has a $(t_{2g})^0$ configuration, and all other metals have a $(t_{2g})^1$ configuration. The second important parameter is the exchange integral, K, which controls the splitting between the various $(t_{2g})^2$ multiplets. In the limit of extreme localization, it is the ratio of these two parameters that is important.[14] As K is an exchange integral and J is a coulomb integral, it is to be expected that K/J will be relatively small. Calculations of K/J for Sc^{I}, Ti^{II}, V^{IV}, Cr^{IV}, and Mn^{V} result in K/J values that range from 0.037 to 0.041.[15] We therefore in this article consider K/J values ranging from 0.0 to 0.1.

(14) In second-order perturbation theory the energy denominator is the difference in energy between the ground and excited states. For the case considered here it can be expressed as $J(1 + mK/J)$ where m is an integer. The J term defines the energy scale leaving K/J as the only parameter.

(15) (a) Watson, R. E. Technical Report No. 12 from Solid State and Molecular Theory Group MIT, Cambridge, Massachusetts, 1959. (b) Watson, R. E. *Dissertation* Thesis, MIT, 1959.

Table V. Ratio of d Block Stabilization Energies for **9**, **11**, and **12**[a]

		H_{loc}	
	$H_{\text{Hückel}}$	$K/J = 0.0$	$K/J = 0.1$
$E(\mathbf{11})/E(\mathbf{9})$	0.91	0.89	0.90
$E(\mathbf{12})/E(\mathbf{9})$	0.82	0.86	0.88

[a] We have set the t_{2g} Hückel coulombic value to zero. Thus the energies reported are the ratio of the total d block stabilization energy caused by t_{2g}–t_{2g} interaction.

Some insight into the $(t_{2g})^1$ localized limit can be found in considering the model system **9**, which is a cluster of four trans edge-sharing octahedra. The 12 t_{2g} orbitals of **9** are shown and named in **10**. For this model system we contrast in Table III

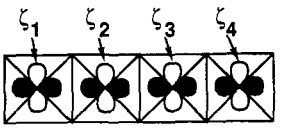

10 a

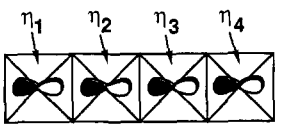

10 b

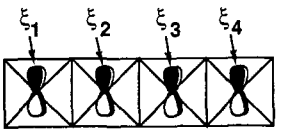

10 c

the localized portion of the Hückel ground state ($P\Psi_{\text{Hückel}}$) with the ground state in the limit of localization for the generalized Hubbard model (Ψ_{loc}). In this preliminary calculation we have eliminated all δ interaction and set $\langle\eta_i|\eta_j\rangle = 0.933\ \langle\zeta_i|\zeta_j\rangle$ where i and j are on neighboring metal atoms. This corresponds to setting $|S_\pi/S_\sigma| = 0.7$. (We discuss and vary these values in latter sections.) As Table III shows, the $P\Psi_{\text{Hückel}}$ provides an excellent estimate for Ψ_{loc} when $K/J = 0.0$ and a reasonable estimate for Ψ_{loc} when $K/J = 0.1$. We may in the same way consider the four transition-metal cluster **11**. The Ψ_{loc} and $P\Psi_{\text{Hückel}}$ are too complicated to present full here (the $S_z = 0$ manifold is a 486-dimensional space!). An excellent measure though is the dot product

$$x = \langle P\Psi_{\text{Hückel}}|\Psi_{\text{loc}}(K/J)\rangle \qquad (9)$$

where $P\Psi_{\text{Hückel}}$ and Ψ_{loc} (K/J) are both normalized. We show these results in Table IV. Recalling that these vectors span a 486-dimensional space, the overlap is really quite large.

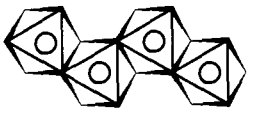

11

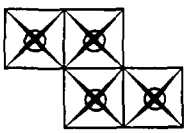

12

We may in the same manner compare the energetic predictions of H_{loc} and $H\Psi_{\text{Hückel}}$. For good measure we also consider the cluster **12**. We show our results in Table V. It may be seen that $H_{\text{Hückel}}$, H_{loc} $(K/J = 0)$, and H_{loc} $(K/J = 0.1)$ all rank the three systems in the same order. The inclusion of electron localization does not alter the energetic predictions. It will be recalled that extended Hückel calculations comparing rutile (**1**) and α-PbO_2 (**2**) suggested that for d^1 configurations the trans arrangement of rutile is lower in energy. To the extent that our four metal clusters form a good estimate of the energetic behavior of the chains **4** and **5**, we conclude that the extended Hückel calculation will correctly predict the $(t_{2g})^1$ structural preferences. As we discussed earlier (see Table II) the Hückel results do correlate

Table VI. S_π/S_σ for Various Metal Atoms

atom	orbital[a]	ζ_1	C_1	ζ_2	C_2	metal–metal[b] distance, Å	S_π/S_σ[c] direct	effective for **9**	effective for **11**
V	3d	4.75	0.4558	1.59	0.7516	2.90	−0.969	−0.431	−0.432
Nb	4d	4.08	0.6401	1.64	0.5516	3.00	−0.986	−0.432	−0.435
Ta	5d	4.76	0.6103	1.94	0.6108	3.07	−0.896	−0.458	−0.452

[a] Double-ζ STO used. [b] Metal distances are average metal–metal distances in MO_2 (M = V, Nb, Ta). [c] S_π/S_σ between atom 1 and atom 2 (see **10**) are given here.

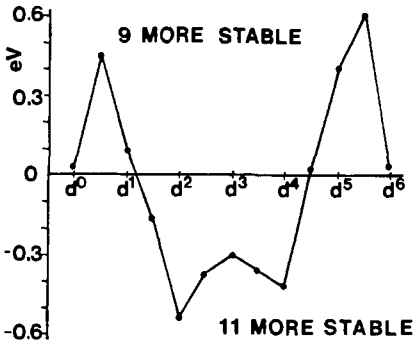

Figure 2. Difference in energy between the trans chain of edge-showing octahedra, **9**, and the cis chain, **11**, as a function of the number of d electrons. Positive values of the curve indicate **9** is more stable, and negative values, that **11** is more stable. Compare with Figure 1.

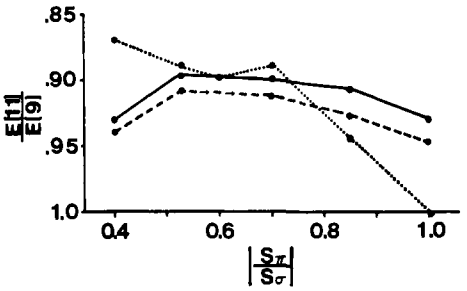

Figure 3. Ratio of stabilization energy of **9** and **11** as a function of $|S_\pi/S_\sigma|$. The y-axis plots the t_{2g} block energy of the ground state of **11** divided by that of **9**. We have set the Hückel coulombic α value equal to zero for the t_{2g} block; thus, energies plotted are ratios of stabilization energies. The dashed line is for $H_{\text{Hückel}}$, and the dotted line, for H_{loc} (K/J = 0.1). Calculations were carried out only at the indicated points.

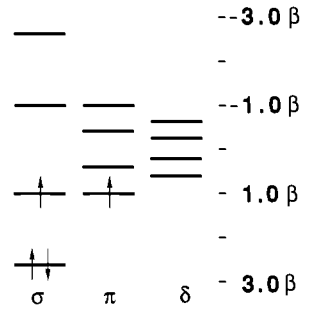

Figure 4. Hückel energy diagram of t_{2g} orbitals of **9** at $|S_\pi/S_\sigma|$ = 0.38. At this critical value, according to Hund's rule a triplet (shown in the figure) would be lower in energy. For $|S_\pi/S_\sigma|$ values either significantly greater or less than this value, the ground state is a singlet.

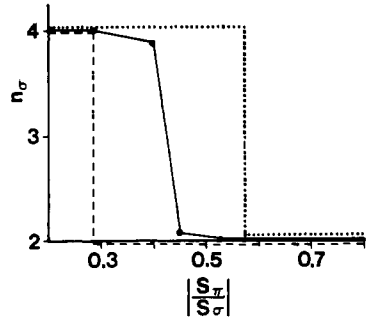

Figure 5. Number of electrons in the lowest lying singlet state as a function of $|S_\pi/S_\sigma|$. H_{loc} (K/J = 0) and solid line for H_{loc} (K/J = 0.1). For this latter curve calculations at four $|S_\pi/S_\sigma|$ ratios were carried out. These are indicated by the points. The solid line is only an aid to the viewer. Furthermore, in the region of transition the Ψ_{loc} (K/J = 0.1) is a triplet where n_σ = 3. See Figure 4.

well with the experimental facts. Are the clusters **9** and **11** though sufficient models for **1** and **2**? One good test is to compare the extended Hückel calculation for these two clusters and compare them with the full band calculation reported by Burdett.[3] We show the relative energies of **9** and **11** in Figure 2. It agrees well with the results shown in Figure 1. We therefore conclude that our calculations are pertinent, as long as the correlated motion of electrons more than four unit cells apart do not give rise to important energetic effects. Finally, we show in Figure 3 that the relative preference of **9** vs **11** is reasonably independent of the value of $|S_\pi/S_\sigma|$.

S_σ and S_π. In the previous section we considered a fixed ratio between the σ overlap S_σ and the π overlap S_π. In Table VI we show the actual value for S_π/S_σ for various transition metals. Two different S_π/S_σ values are given. The direct S_π/S_σ values correspond to the through-space overlap of the transition-metal d orbitals. The effective S_π/S_σ values correspond to a mixture of the through-space and through-bond couplings. We discuss the provenance of these effective S_π/S_σ values in the next section. In this section we discuss the consequences of the various S_π/S_σ numerical values. We consider first **9**. In **9**, the t_{2g} orbitals decompose into a set, which interact principally through σ bonds, purely through δ bonds, and purely through π bonds. We showed these sets in **10**. The Hückel molecular orbital diagram for the composite sets is given in Figure 4. It may be seen that, for a critical value of S_π/S_σ, $\Psi_{\text{Hückel}}$ transforms from a state where all four $(t_{2g})^1$ electrons lie in the σ set, **10a**, to a state where two electrons lie in the σ set and two in the π set, **10b**. The same transition is found to occur when the generalized Hubbard model is used. Indeed when K/J is set equal to zero, it is impossible in the generalized Hubbard model for electrons to leave a σ orbital for a π orbital, and vis-a-versa. Only in the case of a nonzero K/J parameter is such a transition possible. This is so as $(t_{2g})^2$ multiplet configurations contain mixtures of σ and π electrons. In Figure 5 we contrast the change in the number of σ electrons as a function of the S_π/S_σ ratio. We show here the sudden transition that occurs for the Hückel Hamiltonian and for the localized generalized Hubbard model when K/J = 0.0. By contrast the transition is not a step function for K/J = 0.1. It may be seen that while the transition for the Hückel Hamiltonian occurs at a much lower value, the qualitative shape of the function is independent of the asymptotic limit under consideration.

Through-Bond vs Through-Space Interactions. Up to this point we have considered only the direct σ and π transition-metal interactions on neighboring metals. We have therefore neglected the δ bonds and the next nearest neighbor interactions. More importantly we have ignored all through-bond couplings. As the primary interaction is that between the transition metals and its neighboring oxygen anions, in an accurate account of the metal–metal interaction such through-bond coupling must be included. Indeed, much of our understanding of transition-metal interactions in oxides is based on such ideas of superexchange.[5a,12]

Fortunately, it is not difficult to include all these different effects on an equal foooting. We do so in the following manner. In Figure

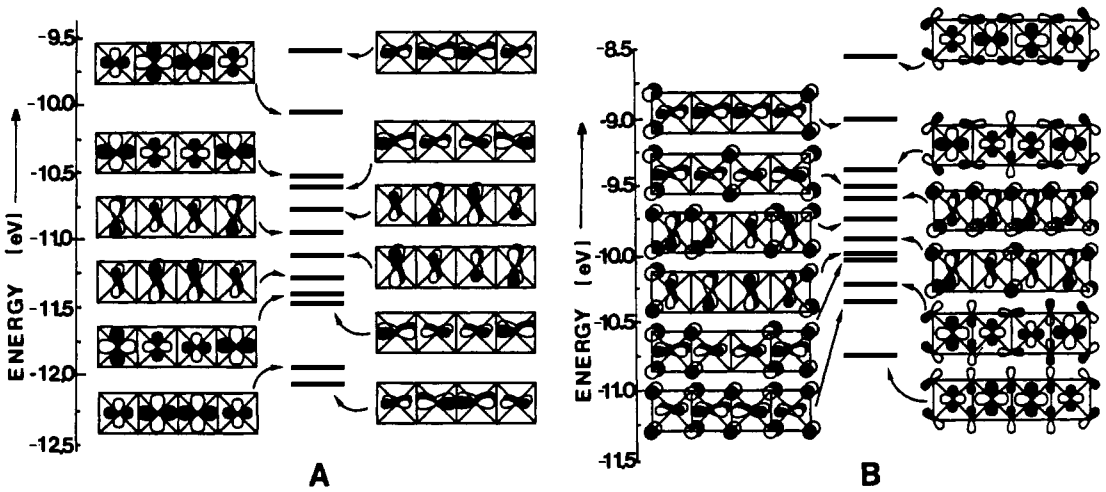

Figure 6. Molecular orbitals (MO's) for the t_{2g} set of **9** in the presence and absence of ligand orbitals. In A we show the MO diagram in the absence of ligand–metal orbital interactions for the purely t_{2g} orbitals. π MO's form both the most bonding and antibonding combination. In B oxygen atoms are also included in the calculation. The size of the oxygen contribution has been enlarged so as to render their phases more clear. Note that the σ MO's now have the strongest interaction. Furthermore, the order of the δ MO's has reversed. In both A and B, calculations were carried out on the geometry described in Table VII.

Table VII. Effective vs Direct Interactions[a]

	effective, eV	direct,[a] eV		effective, eV	direct,[a] eV
		"σ" Block			
$\langle\zeta_1\|H\|\zeta_2\rangle$	−0.681	−0.596	$\langle\zeta_1\|H\|\zeta_3\rangle$	0.054	−0.013
$\langle\zeta_2\|H\|\zeta_3\rangle$	−0.684	−0.577	$\langle\zeta_1\|H\|\zeta_4\rangle$	−0.044	0.033
		π Block			
$\langle\eta_1\|H\|\eta_2\rangle$	0.410	0.758	$\langle\eta_1\|H\|\eta_3\rangle$	0.041	0.074
$\langle\eta_2\|H\|\eta_3\rangle$	0.415	0.765	$\langle\eta_1\|H\|\eta_4\rangle$	0.003	0.007
		δ Block			
$\langle\xi_1\|H\|\xi_2\rangle$	0.119	−0.173	$\langle\xi_1\|H\|\xi_3\rangle$	−0.003	0.003
$\langle\xi_2\|H\|\xi_3\rangle$	0.119	0.173	$\langle\xi_1\|H\|\xi_4\rangle$	0.000	0.000

[a] Perfect octahedra were used in this calculation. Vanadium atoms 2.9 Å apart were chosen. The vanadium parameters were $\alpha(4s) = -8.81$ eV, $\alpha(4p) = -5.52$ eV, $\alpha(3d) = -11.0$ eV. $\zeta(4s) = \zeta(4p) = 1.3$. For V(3d) a double-$\zeta$ expansion was used $\zeta_1 = 4.75$, $C_1 = 0.4558$, $\zeta_2 = 1.5$, $C_2 = 0.7516$. For O, $\alpha(2s) = -32.3$ eV, $\alpha(2p) = -14.8$, $\zeta(2s) = \zeta(2p) = 2.28$. [b] We report here the simple Hückel matrix, which will reproduce the extended Hückel diagram shown in Figure 6A. [c] The σ block contains also a small δ contribution as $\langle\zeta_1|\zeta_2\rangle = {}^3/_4S_\sigma + {}^1/_4S_\delta$.

6 we show the extended Hückel t_{2g} molecular orbital energy diagram for the cluster **9** in both the presence and absence of the surrounding anions. We also include in the former case the transition-metal s and p orbitals. The latter case (i.e., without anions present) shown in Figure 6A corresponds to an ordinary 12-dimensional matrix prroblem. Each of the 12 orbitals are purely t_{2g} in character. By contrast in Figure 6B, where anions have been included, these 12 molecule orbitals, while mainly of t_{2g} character, contain oxygen s and p and to a lesser extent transition metal e_g, s and p character as well. We now introduce an effective Hamiltonian, which has 12 metal t_{2g} orbitals whose interaction exactly reproduces the molecular orbital diagram energies of Figure 6B (see Appendix II for details). In this effective Hamiltonian method we have included implicitly all the through-bond and through-space effects present in the full-valence space extended Hückel calculation. In Table VII we contrast the interactions between these effective orbitals and the more ordinary pure t_{2g} orbitals. In this table we have labeled the 12 orbitals ξ_1 through ζ_4 as shown in **10**. It may be seen that the orbitals conveniently divide into δ, π, and primarily σ blocks. Furthermore, as Table VII shows, there are substantial differences between the direct and the effective interactions. One principle difference is that, in the direct Hamiltonian, π interactions dominate while in the effective approach, σ interactions do so. A second difference is that while for the direct Hamiltonian the δ interaction is positive, for the effective Hamiltonian, it is negative. Both these trends may be seen in Figure 6. The former effect reveals itself in that the π orbitals span the widest range of energies in Figure 6A while the σ orbitals have the widest span in Figure 6B. The interchange of the δ orbital signs may be seen by the reversal of the order of the δ molecular orbitals in going from Figure 6A to Figure 6B.

The cause for these differences may be deduced from Figure 6. The δ interaction reverses sign as it is through-bond (metal–oxygen) coupling, which is of the greatest importance for these molecular orbitals. The oxygen–metal metal interaction though is antibonding rather than bonding, thus leading to a sign reversal in the δ interaction. Similarly, the change in the π and σ bandwidths results from the form of their respective molecular orbitals given in Figure 6B. Whenever the π metal orbitals are antibonding to one another, they are of incorrect symmetry to interact with any oxygen atomic orbitals. This is not the case for π metal–metal bonding orbitals. Recalling that the oxygen–metal interaction is of antibonding character in the t_{2g} block, there is therefore a smaller upward shift for π metal orbitals of metal–metal antibonding character. By contrast for the σ orbitals, the ability of the oxygen orbitals to interact with the transition-metal t_{2g} orbital is independent of whether the transition metals are bonding or antibonding to one another. Hence overall there is a constant shift for all the σ molecular orbitals.

The net result is that, for the effective Hamiltonian interactions, the appropriate S_π/S_σ ratio is much smaller than might have been anticipated. As we have shown in Figure 3, the relative energies of **9** and **11** are reasonably invariant to S_π/S_σ changes (i.e., for S_π/S_σ ranging from 0.4 to 0.9). Indeed when we calculate the energies of the two systems **9** and **11** using the full effective Hamiltonian (which includes second nearest neighbor, δ bonds, and through-bond coupling) our overall answer is not changed by very much. For the vanadium system $E(\mathbf{11})/E(\mathbf{9}) = 0.874$ in reasonable agreement with the results of Figure 3.

Finally we mention two further features of the effective Hamiltonian. It is no longer required that the t_{2g} orbitals on the same atom are orthogonal. Such effects however are slight. Even at their largest they are at least 2 orders of magnitude smaller than the largest overlaps. More significantly, the t_{2g} orbitals no longer have the same α (coulomb) values. For example in **9** the α values of the σ, π, and δ orbitals become, respectively, −9.69, −9.75, and −9.81 eV. This is so as, in the extended Hückel method, atomic orbitals, which strongly interact, give rise to antibonding molecular orbitals, which are more antibonding than the bonding molecular orbitals are bonding. Hence the mean is shifted upward. However, as we are not sure of the validity of this effect, we have censored it from our calculation.

Conclusion

We have shown in this paper that, for certain electron counts (i.e., $(t_{2g})^3$), the energetic predictions of the Hückel model can

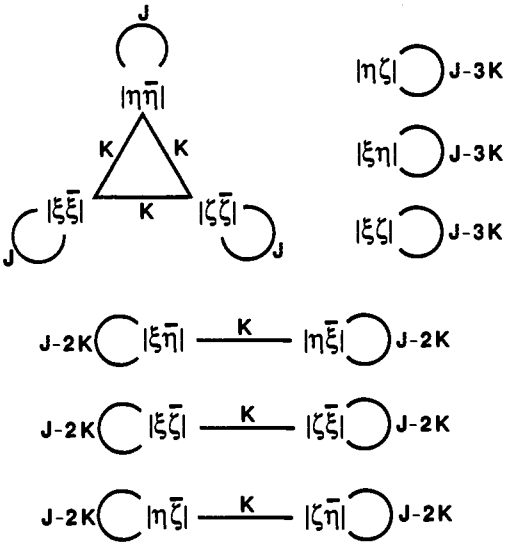

Figure 7. Coulomb and exchange interactions for the $(t_{2g})^2$ configuration. Straight lines represent off-diagonal matrix elements equal to K. Diagonal matrix elements are shown adjacent to the $^3/_4$ circles. Only $S_z \geq 0$ states are shown in this figure.

be completely overturned by the inclusion of the correlated motion of the electrons while for other electron counts (i.e., $(t_{2g})^1$) the Hückel prediction remains consistently valid. Thus is the case of transition-metal systems some care must be taken in applying the extended Hückel results. In the case of $(t_{2g})^3$ systems in which the metals have high formal oxidation states and where the counterion to the metal is highly electronegative, we may anticipate that electron localization is important, and hence the extended Hückel prediction is modified. We have seen that the structural evidence indicates that such is the case for group VIIB oxides and chlorides where the metal is the IV oxidation state. Nevertheless, it should be noted that even for metal ions such as these, there are certain structural questions, such as the question of site preference for which the Hückel answer is still valid.[16] By contrast, much less care needs to be taken for $(t_{2g})^1$ systems. The energetic prediction of the extended Hückel calculation has been shown to be unchanged by electron localization. For this reason the extended Hückel calculation provides an accurate account of the $(t_{2g})^1$ oxide and chloride systems.

Appendix I

Single $(t_{2g})^n$ Configuration. Ignoring both spin–orbit coupling and the effect of any e_g or metal s and p orbital CI, the Tanabe–Sugano term energies[9] and wave functions of both the $(t_{2g})^2$ and $(t_{2g})^3$ configurations correspond to the Hamiltonian shown diagrammatically in Figure 7. We follow in this figure and throughout this paper the Tanage–Sugano nomenclature[9] where ξ, η, and ζ stand for, respectively, the yz, xz, and xy t_{2g} orbitals. The J and K of Figure 7 are the standard two electron integrals:

$$J = \int d\vec{r}_1\, d\vec{r}_2\, \zeta^*(\vec{r}_1)\xi^*(\vec{r}_2)\frac{1}{|\vec{r}_1 - \vec{r}_2|}\zeta(\vec{r}_1)\zeta(\vec{r}_2) \qquad (10)$$

$$K = \int d\vec{r}_1\, d\vec{r}_2\, \xi^*(\vec{r}_1)\xi^*(\vec{r}_2)\frac{1}{|\vec{r}_1 - \vec{r}_2|}\zeta(\vec{r}_1)\zeta(\vec{r}_2) \qquad (11)$$

It may be seen, from Figure 7, that the illustrated Hamiltonian is the same as that discussed by Tanabe, Sugano, and Kamimura.[9] It corresponds to the Hamiltonian

$$H_1 = \sum_{\substack{i,j \\ m,n}} \frac{K}{2}\{a^+_{jnl}a^+_{jml}a_{imlA}a_{inl} + a^+_{jnl}a^+_{imlA}a_{jml}a_{inl}\} + \frac{J-2K}{2}\{a^+_{jnl}a^+_{imlA}a_{imlA}a_{jnl}\} \qquad (12)$$

(16) Lee, S. *J. Am. Chem. Soc.* **1988**, *110*, 8000.

Multi-$(t_{2g})^n$ Configurations. Our interest is in exploring the effect of metal–metal interactions. We assume that the Hückel β interactions are the predominant interaction of this type. We therefore choose for our generalized Hubbard Hamiltonian

$$H_{gH} = \sum_l H_l + \sum_{\substack{j,l,j' \\ l,m}} \beta_{jl,j'l'}a^+_{jlm}a_{j'l'm} \qquad (13)$$

Our primary interest in H_{gH} is in contrasting localized to delocalized electronic behavior. Delocalized motion, which corresponds to molecular orbital theory is to be found when J and K are small in comparison to the principal β interactions. Localized motion corresponds to the limit where J and K are large compared to all β interactions. Furthermore, as we are not at present interested in studying mixed-valence species, we assume $J \gg K \gg |\beta_{jl,j'l'}|$. As J is the dominant term, we therefore find that the last term in eq 12 dominates. As J is always positive it may be seen that the lowest energy configurations have (to the extent it is possible) a uniform number of electrons on each metal site.

$(t_{2g})^3$ Configuration. In the case where every metal atom is of the $(t_{2g})^3$ type, eq 13 can be simplified. We consider here the regime where $J \gg K \gg |\beta_{jl,j'l'}|$. The ground state of H_1 under these conditions is just the quadruplet $^4A_{1g}$. In the $^4A_{1g}$ multiplet the ξ, η, and ζ t_{2g} orbitals are each singly occupied. As the K interaction has been assumed large compared to the β interactions, we need therefore consider as our low-lying states only those states that have each t_{2g} orbital singly occupied. The first term of eq 12 (out of the three terms) applies only to doubly occupied t_{2g} orbitals and may therefore be ignored (for lowest order perturbation correction). The last term is merely an additive constant dependent on the number of t_{2g} electrons. H_1 therefore reduces to

$$H_1 = \sum_{\substack{i,j \\ m,n}} \frac{K}{2}a^+_{jnl}a^+_{imlA}a_{jmlA}a_{inl} + C(N_1) \qquad (14)$$

$$C(N_1) = \begin{cases} J - 2K & N_1 = 2 \\ 3(J-2K) & N_1 = 3 \\ 6(J-2K) & N_1 = 4 \end{cases} \qquad (15)$$

and N_1 is the number of t_{2g} electrons on the lth site. This may be written in a spin operator form

$$H_1 = \sum_{i>j} \frac{K}{2}(1 - 4\vec{S}_{il}\vec{S}_{jl}) + C(N_1) \qquad (16)$$

where $\vec{S}_{il}$ is a spin $^1/_2$ operator of the ith t_{2g} orbital of the lth atom [e.g., $S_{\xi l-}$ operator is the lowering that converts ξ_l into $\bar{\xi}_l$]. Therefore, we find:

$$H_{gH} = \sum_{\substack{i,j \\ l}} \frac{K}{2}(1 - 4\vec{S}_{il}\vec{S}_{jl}) + C(N_1) + \sum_{\substack{jl,j'l' \\ m}} \beta_{jll'l'}a^+_{jlm}a_{j'l'm} \qquad (17)$$

Treating the interatomic interactions as a perturbation, we find that the second-order perturbed form of H_{gH} is:

$$H_{gH} = \sum_{i>j} \frac{K}{2}(1 - 4\vec{S}_{il}\vec{S}_{jl}) - \frac{1}{J-2K}\sum_{\substack{j,l \\ j',l'}}(\beta_{jll'l'})^2(1 - 4\vec{S}_{jl'}\vec{S}_{j'l'}) \qquad (18)$$

We therefore have, as might be expected, a strong intraatomic ferromagnetic interaction and a weaker antiferromagnetic interatomic interaction. As we have assumed a $(t_{2g})^3$ configuration at each atom, we can express the above in terms of $^3/_2$ spin operators S_l

$$H_{gH} = \sum_{l,l'} L_{ll'}\vec{S}_l\vec{S}_{l'} + \text{constant} \qquad (19)$$

where

$$L_{ll'} = \frac{4}{J-2K}\sum_{j,j'}(\beta_{jll'l'})^2\frac{1}{9} \qquad (20)$$

This is the result used in the text.

Appendix II

Our effective Hamiltonian is made by the following recipe. We project the 12 t_{2g} molecular orbitals onto the pure t_{2g} atomic orbital space. Let us call these projected orbitals $Q\Psi_n$ where n ranges from 1 to 12 and where

$$H_{eH}\Psi_n = \lambda_n\Psi_n \quad (21)$$

We require

$$H'_{eff}Q\Psi_n = \lambda_n Q\Psi_n \quad (22)$$

H'_{eff} is not a hermetian operator. Therefore we define

$$H_{eff} = \frac{1}{2}(H'_{eff} + H'^{T}_{eff}) \quad (23)$$

It should be noted that the deviation of H'_{eff} from hermeticity has been found to be very slight.

The Unimolecular Triple Dissociation of Glyoxal: Transition-State Structures Optimized by Configuration Interaction and Coupled Cluster Methods

Gustavo E. Scuseria† and Henry F. Schaefer III*

Contribution No. 50 from the Center for Computational Quantum Chemistry, School of Chemical Sciences, University of Georgia, Athens, Georgia 30602. *Received March 24, 1989*

Abstract: Several high-level ab initio theoretical methods have been used to investigate the proposed (1980) "triple whammy" mechanism for the unimolecular dissociation of glyoxal. Basis sets of double zeta plus polarization (DZ+P) and triple zeta plus double polarization (TZ+2P) quality have been used in connection with CISD, CCSD, and CCSDT-1 theoretical methods. The theoretical studies show unambiguously that the triple dissociation mechanism is operative under conditions used in the laboratory to investigate glyoxal photochemistry. Also confirmed, contrary to existing experiments, is the early (1975) theoretical prediction of Dykstra that the C–C single bond distance of *cis*-glyoxal is longer than for *trans*-glyoxal. Vibrational frequencies for both *cis*- and *trans*-glyoxal are predicted and show good qualitative agreement with existing experimental data. The ordering (theory and experiment) of cis and trans C–C stretching frequencies is consistent with the theoretical structural predictions. The predicted energy difference between the cis and trans isomers of glyoxal falls within the error bars of the recent experiments by Parmenter's group.

Prior to 1981 it was generally agreed, following pioneering work by Parmenter,[1] that the photodissociation of glyoxal[2] to give molecular hydrogen proceeded via the two-step mechanism

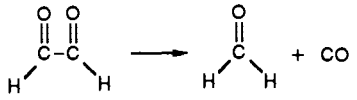

(1a)

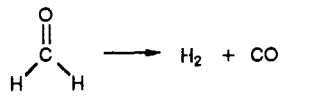

(1b)

However, in 1981 Osamura and one of us (OS)[3] pointed out that the large barrier height for formaldehyde dissociation (eq 1b) precludes this two-step mechanism under typical conditions for glyoxal dissociation. Based on qualitative molecular orbital theory (Woodward–Hoffmann-like orbital correlation diagrams), OS suggested in place of (1) the unimolecular triple dissociation mechanism

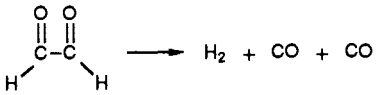

(2)

The unconventional "triple whammy" proposal of OS[3] was subjected to quantitative theoretical examination later the same year by Osamura, one of us, Dupuis, and Lester (OSDL).[4] OSDL optimized the glyoxal stationary point structures at the self-consistent-field (SCF) level of theory, using basis sets as large as double zeta plus polarization (DZ+P). However, correlation effects were considered only at assumed geometries with the much smaller 3-21G basis set.[5] The Davidson-corrected[6] CISD (configuration interaction including all single and double excitations) barrier height for (2) is predicted to be 66 kcal/mol with the 3-21G basis set. OSDL[4] argued in addition that the effects of zero-point vibrational energy (ZPVE) would place the triple whammy activation energy below the experimental upper bound of 62.9 kcal. Thus the hypothesized[3] unimolecular triple dissociation gained substantial theoretical support.

The experimental upper bound to the activation energy requires a brief explanation. The glyoxal photodissociation experiments typically begin with the laser-excitation of ground-state-*trans*-glyoxal, S_0, to the zero-point vibrational level of the first excited singlet state, S_1. This zero-point level of S_1 is known to lie 62.9 kcal above the vibrational ground state of S_0 *trans*-glyoxal. Thereafter, there occurs a radiationless transition

$$S_1 \rightarrow S_0$$

to the upper vibrational manifold of the ground-state S_0 potential energy surface. The Hepburn experiments[7] show that dissociation

† Present address: Department of Chemistry, Rice University, P.O. Box 1892, Houston, TX 77251.

(1) Parmenter, C. S. *J. Chem. Phys.* **1964**, *41*, 658.
(2) For early work on the photochemistry of glyoxal, see: Norrish, R. G. W.; Griffiths, J. G. A. *J. Chem. Soc.* **1928**, 2829. Thompson, H. W. *Trans. Faraday Soc.* **1940**, *36*, 988. Calvert, J. G.; Layne, G. S. *J. Am. Chem. Soc.* **1953**, *75*, 856.
(3) Osamura, Y.; Schaefer, H. F. *J. Chem. Phys.* **1981**, *74*, 4576.
(4) Osamura, Y.; Schaefer, H. F.; Dupuis, M.; Lester, W. A. *J. Chem. Phys.* **1981**, *75*, 5828.
(5) Binkley, J. S.; Pople, J. A.; Hehre, W. J. *J. Am. Chem. Soc.* **1980**, *102*, 939.
(6) Davidson, E. R. In *The World of Quantum Chemistry*; Daudel, R., Pullman, B., D. Reidel: Dordrecht, Holland, 1974.
(7) Hepburn, J. W.; Buss, R. J.; Butler, L. J.; Lee, Y. T. *J. Phys. Chem.* **1983**, *87*, 3638.

0002-7863/89/1511-7761$01.50/0